Folding Then Binding vs Folding Through Binding in Macrocyclic Peptide Inhibitors of Human Pancreatic α-Amylase

Leander Goldbach,[‡,#] Bram J. A. Vermeulen,[†,#] Sami Caner,[§,#] Minglong Liu,[○] Christina Tysoe,[⊥,‖] Lieke van Gijzel,[○] Ryoji Yoshisada,[○] Mikael Trellet,[‡] Hugo van Ingen,[†] Gary D. Brayer,[§] Alexandre M. J. J. Bonvin,[‡] and Seino A. K. Jongkees*,[○]
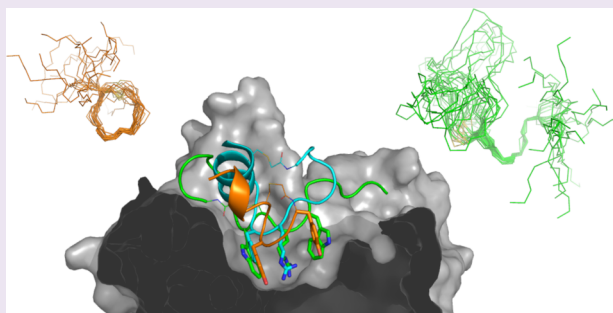
[†]NMR Spectroscopy Research Group and [‡]Computational Structural Biology, Bijvoet Center for Biomolecular Research, Science Faculty, Utrecht University, 3512 Utrecht, The Netherlands

[§]Department of Biochemistry and Molecular Biology, [⊥]Centre for High-Throughput Biology, and [‖]Department of Chemistry, University of British Columbia, Vancouver, BC V6T 1Z4, Canada

[○]Department of Chemical Biology and Drug Discovery, Utrecht Institute of Pharmaceutical Sciences, Utrecht University, 3584 CG Utrecht, The Netherlands

S *Supporting Information*

ABSTRACT: *De novo* macrocyclic peptides, derived using selection technologies such as phage and mRNA display, present unique and unexpected solutions to challenging biological problems. This is due in part to their unusual folds, which are able to present side chains in ways not available to canonical structures such as α-helices and β-sheets. Despite much recent interest in these molecules, their folding and binding behavior remains poorly characterized. In this work, we present cocrystallization, docking, and solution NMR structures of three *de novo* macrocyclic peptides that all bind as competitive inhibitors with single-digit nanomolar K_i to the active site of human pancreatic α-amylase. We show that a short stably folded motif in one of these is nucleated by internal hydrophobic interactions in an otherwise dynamic conformation in solution. Comparison of the solution structures with a target-bound structure from docking indicates that stabilization of the bound conformation is provided through interactions with the target protein after binding. These three structures also reveal a surprising functional convergence to present a motif of a single arginine sandwiched between two aromatic residues in the interactions of the peptide with the key catalytic residues of the enzyme, despite little to no other structural homology. Our results suggest that intramolecular hydrophobic interactions are important for priming binding of small macrocyclic peptides to their target and that high rigidity is not necessary for high affinity.

Macrocyclic peptides are a class of molecule currently generating substantial interest both from academic researchers and the pharmaceutical industry. These molecules, with their large available interaction surface area and many potential contacts, are able to bind diverse protein targets with high affinity and selectivity. This, coupled with the increase in stability that typically arises from peptide macrocyclization, has stimulated developments in technology for generating cyclized variants of known interacting peptides. Such a rational approach has had many successes,[1−3] particularly for protein−protein interactions, but it is focused largely on the canonical protein secondary structure elements, in particular α-helices or short antiparallel β-sheets. These folds are useful in cases where the peptide is derived from an interacting part of another protein, but the class of macrocyclic peptides can be much more broad in its structural landscape.

Noncanonical folds are able to access a much broader range of side-chain presentations, and so should be able to bind to a much broader range of protein targets. Peptide display technologies, such as phage or mRNA display, can be coupled with bio-orthogonal macrocyclization reactions to provide another source of macrocyclic peptides, a *de novo* source that is not limited to canonical folds and which allows discovery of peptides directly in macrocyclic form.[4] The few reported structures for these *de novo* macrocyclic peptides reveal a much broader conformational landscape,[5,6] and these display technologies have proven themselves to be a reliable source of ligands for otherwise challenging biological problems such as protein−protein interactions[7,8] or isoform-selective inhibition.[9,10] Despite these successes, little is known at present about the conformational stability and folding behavior of *de*

novo macrocyclic peptides, either bound to their targets or free in solution.

The current advantage in rational design and optimization of the canonical folds is decades of research into understanding their folding and stability requirements, allowing reliable conversion of a linear precursor sequence of biological origin into a macrocyclic variant.[11,12] For example, α-helices can be stabilized through hydrocarbon stapling of the *i* and *i* + 4 or *i* + 7 residues, provided this staple does not otherwise interfere with the binding interface. It remains unclear to what extent the same principles for stabilization can be applied to *de novo* macrocyclic peptides, or whether a well-defined conformation in solution is necessary for binding with high affinity.

In this work we assess the inhibitory properties of several macrocyclic peptides selected against human pancreatic α-amylase (HPA) and through characterization and comparison of several target-bound and solution structures illustrate some unusual patterns of folding behavior that distinguishes the class of *de novo* macrocyclic peptides from the paradigm of stapled canonical folds.
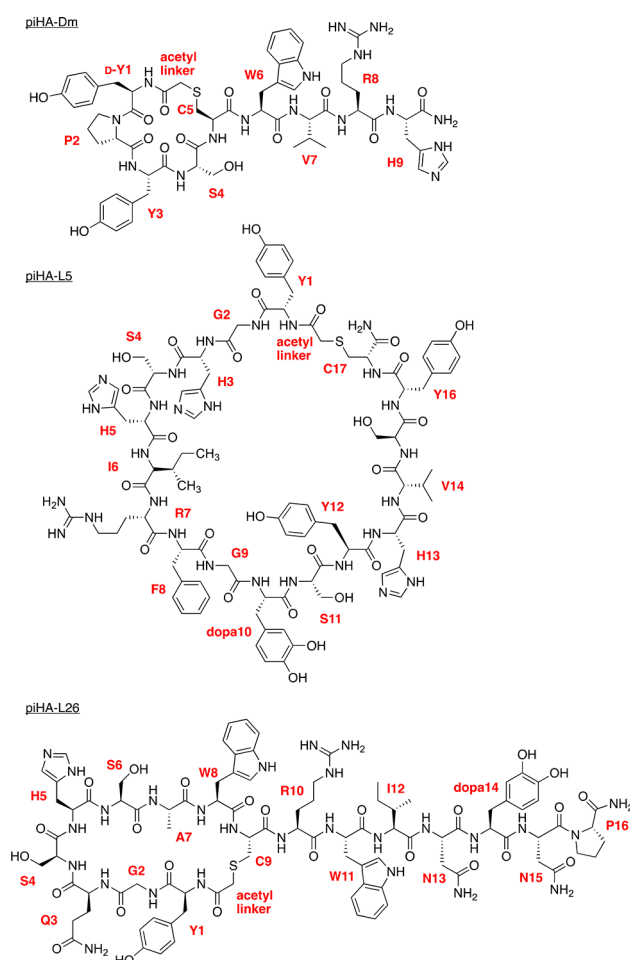
■ RESULTS AND DISCUSSION

Selected Macrocyclic Peptides are Nanomolar Inhibitors of Human Pancreatic α-Amylase. Recently we reported an mRNA display-based selection for peptides binding to HPA.[13] A pair of random macrocyclic peptide libraries was generated by using *N*-chloroacetylated L- and D-tyrosine as initiating amino acids in the RaPID system.[14] The D-tyrosine initiated library was characterized in this previous work and revealed a set of highly conserved sequences we termed peptide inhibitors of human amylase (abbreviated to "piHA"), from which we arrived at a 9 amino acid lariat peptide (piHA-Dm, Scheme 1) that exhibited exemplary potency and selectivity in its inhibition. The library initiated with L-tyrosine, however, remained largely unstudied and sequencing data (Figure S1) hinted at much greater diversity in the possible sequences, and therefore structures, that could bind to this enzyme.

Synthesis and testing of peptide sequences covering representatives of the main consensus motif from this L-tyrosine initiated library (-RFGYAY-; piHA-L1, L3, and L5 numbering represents relative sequence abundance), as well as several other sequences that have clear differences from it (piHA-L12 and L26), showed these to be high affinity competitive inhibitors of HPA, with potency in the low nanomolar range (Table 1, Scheme 1). Truncations of the lariat sequence piHA-L26 showed that the N-terminal macrocycle "head" and the beginning of the C-terminal linear "tail" are crucial for binding.

The amino acid L-dopa (abbreviated here as "d") was present in several of these sequences, being incorporated in the mRNA displayed library as a potential mimic of a recently described natural product that forms a tight chelating interaction with the catalytic residues of this enzyme.[15] In piHA-Dm, incorporation of this residue provided an order-of-magnitude increase in potency through interaction with an active site carboxylate,[16] but in these L-tyrosine initiated sequences this residue was found to have less impact on binding (see piHA-L26 and piHA-L5, and their L-dopa to tyrosine variants), suggesting that in these sequences L-dopa is not placed appropriately in the active site to bind in a similar manner. Substitution of phenylalanine in the consensus motif with tyrosine, which was present at this position in a

Scheme 1. Structures of piHA-Dm, piHA-L5, and piHA-L26

subpopulation of the sequences found, also did not lead to substantially improved binding (see piHA-L3, and its F8Y variant). Unexpectedly and in contrast to all of the other peptides, this variant showed incomplete inhibition even at relatively high peptide concentrations (5 μM). This is inconsistent with the initial characterization of these as competitive inhibitors, as further verified by the crystal structure of piHA-L5(d10Y) described below, and we have no explanation for this result. These L-tyrosine initiated peptides are thus potent inhibitors of HPA and appear to employ a different mode of interaction from our previously reported macrocyclic peptide inhibitor.

Cocrystal Structure of piHA-L5(d10Y) Shows Binding Across the Active-Site Pocket as an Alpha Helix. To investigate what interactions the consensus motif -RFGYAY- is making with the HPA active site, cocrystallization was attempted for several of these homologues with HPA, and an X-ray cocrystal structure eventually solved with piHA-L5(d10Y) bound (Figures 1 and S2). This structure revealed that the peptide forms two turns of an α-helix spanning the enzyme active site pocket, with the consensus motif present partially in the N-terminus of this helix and with the remainder on a loop connecting the two termini. The invariant glycine residue in the consensus motif appears to prevent a steric clash with the enzyme and the highly conserved arginine makes a charge interaction with HPA Glu233 (catalytic acid/base; in this work three letter codes are used for enzyme residues and one letter codes for peptide residues), while the remainder of

Table 1. HPA Inhibition Potency for Macrocyclic Peptides under Study and Their Variants[a]

peptide	sequence	potency (K_i, nM)
piHA-L1	cyclo(Ac-YPTKRYGQWLPYRNNNC)G-NH$_2$	1.7 ± 0.4
piHA-L3	cyclo(Ac-YWDRPTRFGYAYSVIYC)G-NH$_2$	3.0 ± 0.7
piHA-L5	cyclo(Ac-YGHSHIRFGdSYHVSYC)G-NH$_2$	2.8 ± 0.7
piHA-L12	cyclo(Ac-YTFRDWRRSYGGITVRC)G-NH$_2$	9.2 ± 4.0
piHA-L26	cyclo(Ac-YGQSHSAWC)RWINdNP-NH$_2$	8.7 ± 2.6
piHA-L3(F8Y)	cyclo(Ac-YWDRPTRYGYAYSVIYC)G-NH$_2$	10.2 ± 2.7[c]
piHA-L5(d10Y)[b]	cyclo(Ac-YGHSHIRFGYSYHVSYC)G-NH$_2$	14.3 ± 4.2
piHA-L26(d14Y)	cyclo(Ac-YGQSHSAWC)RWINYNP-NH$_2$	2.7 ± 0.7
piHA-L26-Δ14	cyclo(Ac-YGQSHSAWC)RWIN-NH$_2$	3.5 ± 0.6
piHA-L26-Δ10	cyclo(Ac-YGQSHSAWC)-NH$_2$	(≫5000)
piHA-L26(9−17)	Ac-RWINYNP-NH$_2$	(≫5000)

[a]Conserved motifs are underlined. [b]d = L-dopa. [c]Incomplete inhibition.
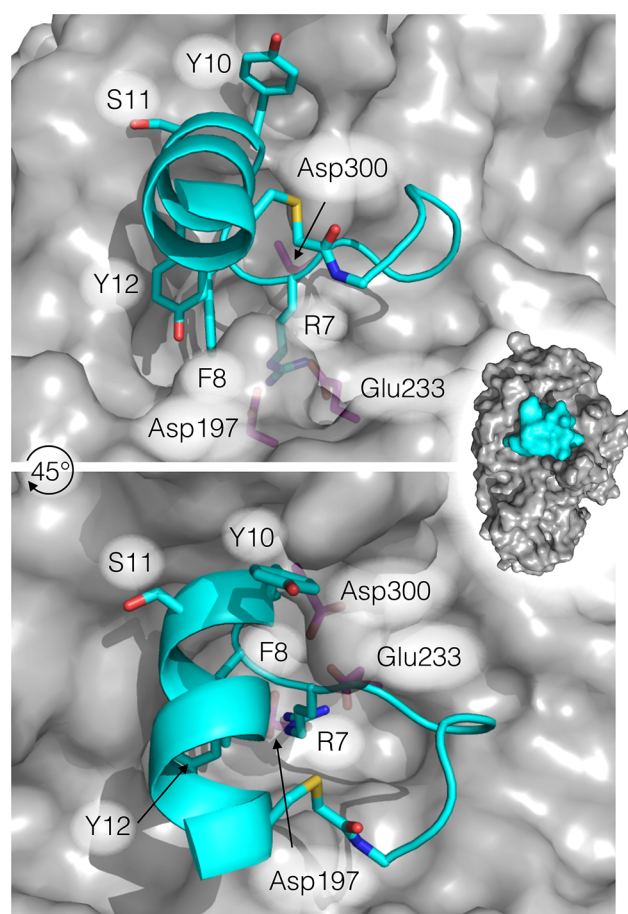

Figure 1. Co-crystal structure of piHA-L5(d10Y) with human pancreatic α-amylase, showing the backbone as a cartoon and the side chains of the consensus motif as sticks. In cyan is the peptide, in gray the protein surface, and in magenta the key catalytic residues. Heteroatoms are colored blue for nitrogen, red for oxygen, and yellow for sulfur. Amylase residues are labeled with three-letter codes, and peptide residues with one-letter codes. (inset) Model of the entire protein−peptide interaction surface (PDB 5VA9).

the motif binds along the wall of the active site pocket. This mode of interaction is different from that shown by piHA-Dm (Figure S3), where interaction of a pair of tyrosines with the active site pocket provided the largest contributions to binding.[13] While this piHA-L5(d10Y) peptide does contain two tyrosine residues with similar spacing to that seen in piHA-Dm, their roles are clearly not the same, consistent with the

effects seen for variants of these residues (Table 1). Overall these two structures share little to no similarity, but it is notable that this is the second observation of an alpha helical segment in a *de novo* macrocyclic peptide.[17] Also of note is that binding of this peptide causes substantial conformational restriction in the amylase protein, as assessed by normalized b-factor in the bound and unbound states (Figure S4). This is not unexpected, given the extensive contacts formed, but does indicate that these macrocyclic peptides could be expected to give substantial thermal stabilization to the target protein. Notably, several macrocyclic peptides derived from the RaPID system have been shown to improve crystallization of membrane proteins.[18]

Docking of piHA-L26-Δ14 Reveals an Extended Conformation with Unusual Secondary Structure. In contrast to the consensus sequence found in piHA-L5(d10Y), the lariat peptide piHA-L26 was present at relatively low abundance in our sequencing results, despite being of equal or higher potency to the other sequences found. Its divergent sequence piqued our interest, and several attempts were made to either cocrystallize this with HPA or to soak it into existing crystals. Despite our efforts, including with truncated peptides, no structure could be solved (see Supplementary Information). We opted for a computational alternative, using the information-driven docking software HADDOCK[19] to dock the peptide. As a pool of starting points for this process we used *ab initio* estimates of plausible solution structures generated by several different online peptide structure prediction tools (Figure S5), but given that these do not accurately account for the thioether cyclization, we do not necessarily expect these to accurately predict the solution structure.

This approach generated several clusters of models, some with the active site interacting with the linear tail and others with a part of the macrocycle (Figure S6). Notable in some of these models (clusters 4 and to a lesser extent 3) is an interaction between R10 and Glu233, very similar to that seen in the piHA-L5(d10Y) structure. In a subset of these models either W8 or W11 were found to be positioned adjacent to the arginine. In other models (clusters 6 and 3) it was residue Y1 that scored highly in interaction energy. Synthesis of peptides with variants of these highest-scoring residues provided a means of assessing the models (Table 2). The Y1A variant showed a substantial decrease in inhibition but much less of a decrease than the W8A, R10A, and W11A variants. Tyrosine substitutions at the aromatic positions showed recovery of most of the inhibition potency. This indicates that both

Table 2. Inhibition Potency of piHA-L26 Variants Testing the Enzyme-Docked Models[a]

peptide	sequence	potency (IC_{50}, nM)
piHA-L26-(d14Y, Y1A)	cyclo(Ac-**A**GQSHSAWC) RWINYNP-NH$_2$	210 ± 50
piHA-L26-(d14Y, W8A)	cyclo(Ac-YGQSHSA**A**C) RWINYNP-NH$_2$	2700 ± 700
piHA-L26-(d14Y, W8Y)	cyclo(Ac-YGQSHSA**Y**C) RWINYNP-NH$_2$	72 ± 15
piHA-L26-(d14Y, R10A)	cyclo(Ac-YGQSHSAWC) **A**WINYNP-NH$_2$	6000 ± 1400
piHA-L26-(d14Y, W11A)	cyclo(Ac-YGQSHSAWC) R**A**INYNP-NH$_2$	3900 ± 800
piHA-L26-(d14Y, W11Y)	cyclo(Ac-YGQSHSAWC) R**Y**INYNP-NH$_2$	170 ± 40

[a]Parent sequence K_i = 2.7 nM, with changes emphasized in bold.

tryptophans and the arginine form the core of the interaction, with cluster 4 coming closest to representing this, but no single model from the first round of docking seemed to accurately capture this experimental result.

These results were then used to guide a subsequent round of model refinement, wherein both tryptophan residues were made active in the HADDOCK framework, meaning they must form interactions with the protein. The highest scoring model from this (Figure 2) appeared to fit the substitution and truncation results (Tables 1 and 2). In this model, the arginine side chain is located in the same position as R7 of piHA-L5(d10Y), while the tryptophans are found in the same locations as the aromatic rings of $^DY1$ and Y3 of piHA-Dm, as well as residue F8 of piHA-L5(d10Y). The macrocycle binds largely adjacent to the active site pocket, with the N-terminal end of the tail entering into the active site in a distinctive turn conformation to bring W8 and R10 together. The end of the tail extends into solution, consistent with the permitted truncation of the last three amino acids and also the location of the covalent mRNA tag in the original selection. This model shows little to no homology with any other previous structures of HPA-inhibiting peptides beyond the placement of the key arginine and tryptophan side chains. While we can be reasonably certain of the roles of these interacting amino acids given the corroborating evidence, the exact placement of all other residues and the backbone as a whole is less certain. It is also possible that the peptide retains significant flexibility while bound, which could rationalize the crystallization problems.

The apparent convergence of side-chain positioning among these different inhibitors (Figure 3) suggests it is a particularly privileged interaction motif for this active site. Indeed, a nearly identical motif (-WRY-) is present in a well-studied protein inhibitor of this same enzyme, Tendamistat.[20] This 74 amino acid protein binds with low picomolar affinity[21] and has been the target of several attempts at rational mimicry.[22,23] Despite not aiming for such a motif, our small macrocyclic peptides appear to successfully capture some or most of the same interactions as Tendamistat, using scaffolds such as the discontinuous motif in piHA-L26 that likely never would have been attempted by rational design. This illustrates well the power of selection systems in finding unexpected solutions to the challenges posed by binding to an enzyme active site.

NMR Solution Structures of piHA-L26-Δ14 and piHA-Dm Suggest That These Peptides Fold through Binding. With canonical folds such as the α-helix seen in piHA-
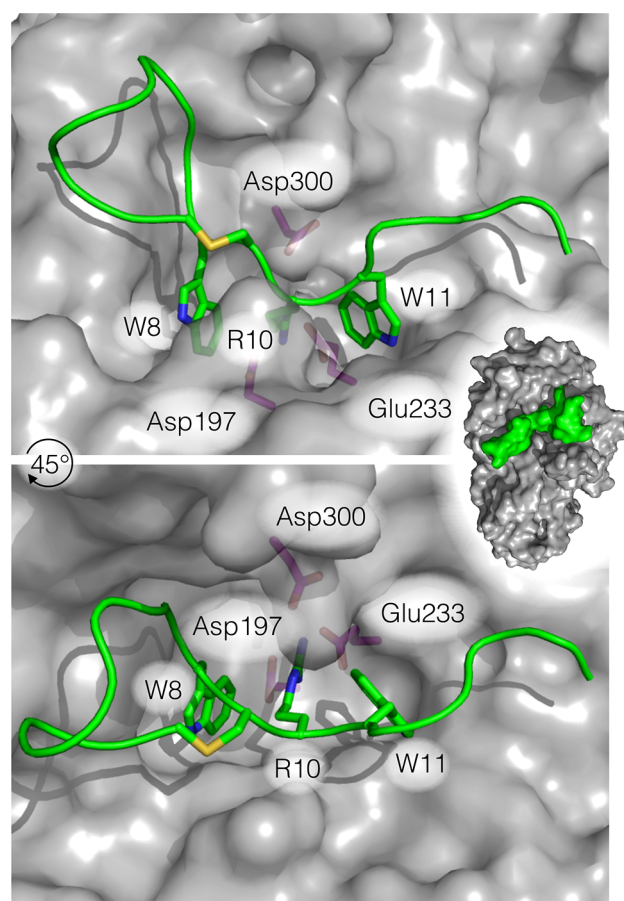

Figure 2. Model of piHA-L26-Δ14 docked in the active site of human pancreatic α-amylase, showing the peptide backbone as a cartoon and the side chains of W8, R10, and W11 as sticks. Color and numbering schemes are as for Figure 1, with piHA-L26(d14Y) shown in green. (inset) Model of the entire protein−peptide interaction surface.
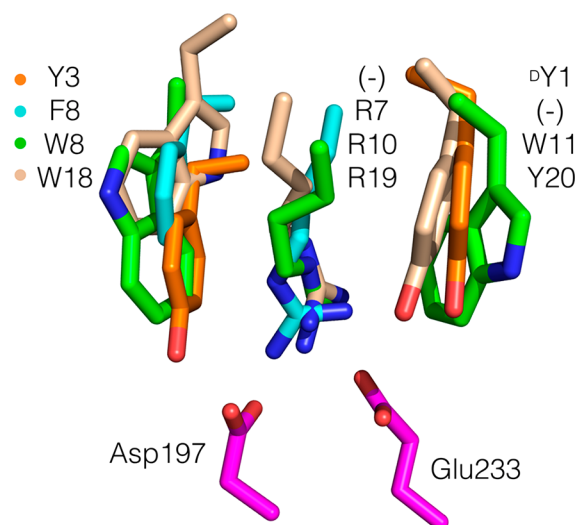

Figure 3. Overlay of the key residues of piHA-Dm (orange), piHA-L5(d10Y) (cyan), piHA-L26-Δ14 (green), and Tendamistat (wheat), interacting with human pancreatic α-amylase catalytic residues (magenta); all shown as sticks. Amino acid side-chains in each subsite are listed in the same order, with (−) indicating no residue in that position from a given peptide.

L5(d10Y), the existence of stable conformations in solution is well established.[11,12] Macrocyclic peptide inhibitors of protein−protein interactions derived from natural interaction partners typically attempt to stabilize a folded conformation in solution to follow a "fold then bind" pattern. For noncanonical folds, which appear to be common in *de novo* macrocyclic peptides, it is not at all clear if these can fold stably in solution, and thus also whether or not the same "fold then bind" pattern is followed. Two of the piHA structures reported, piHA-Dm and piHA-L26, have revealed two very different noncanonical folds in their target-bound structures; a macrocycle-templated 3_{10}-helix and a more extended conformation with a turn presenting the critical interacting residues. To investigate how peptide folding and dynamics may be involved in target binding, we solved the solution structure for the most potent variant of each of these peptides in their free state by NMR spectroscopy.

For piHA-Dm(Y 3d), the NMR chemical shifts, coupling constants and NOE data all point to a highly flexible peptide, in particular in the C-terminal tail. No medium- or long-range NOEs were observed under a variety of conditions. This is reflected in the solution structure of piHA-Dm(Y 3d) showing a disordered tail connected to the N-terminal macrocycle (Figure 4A). Analysis of NMR ^{13}C chemical shifts, however,
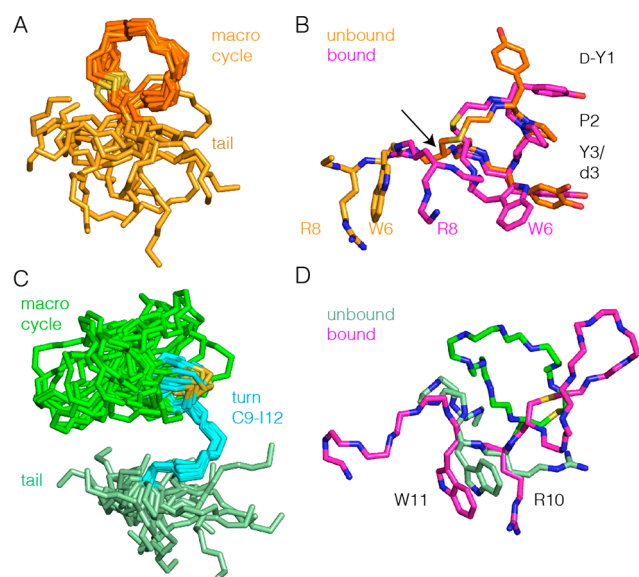

Figure 4. (A) 20 lowest energy conformations of piHA-Dm based on solution NMR constraints, showing the backbone conformation aligned on the macrocycle. (B) Comparison of free piHA-Dm(Y 3d) to the piHA-Dm bound-state crystal structure (PDB: 5KEZ), with selected side chains labeled and color coding as indicated in the figure. The arrow points to the different tail-ring orientation. (C) 20 lowest energy conformations of piHA-L26(d14Y) based on solution NMR constraints, overlaid based on the turn formed by C9−I12. (D) Comparison of the free and target-docked structure, with selected side chains labeled. Cys sulfur atom shown in yellow in all panels.

indicates a propensity for the tail to transiently fold into a helical conformation (Figure S7). The backbone of the ring appears relatively ordered, as may be expected for a constrained five amino acid macrocycle. This results in the free and target-bound states exhibiting similar presentation of the D-tyrosine and L-dopa residues that make critical interactions with the enzyme active site (Figure 4B). There is a marked difference in the relative orientation of the tail

backbone between free and bound structures, which impacts the presentation of the important W6 and R8 side chains (Figure S8). We previously reported a CD spectrum of piHA-Dm that was consistent with formation of a 3_{10}-helix as evidence of folding of the C-terminal tail in solution.[16] Given the inherent instability of a 3_{10}-helix, transient folding and unfolding seems more likely than constitutive folding. This unusual fold may be beneficial for binding, allowing optimization of contacts that would otherwise be strained by the more constitutively stable α-helical fold.

For piHA-L26(d14Y), the NMR data similarly indicate that the peptide is flexible and does not contain stable canonical secondary structure elements (Figure S9). Several medium and long-range NOEs were observed, however, pointing to the presence of a folded "core" formed by side chains of Y1, Q3, W8, and C9 in the macrocycle and I12 in the tail (Figure S10). The solution structure shows a well-defined turn formed by residues C9 through I12, encompassing the first few residues of the tail (Figure 4C). This turn is stabilized by the above-mentioned "hydrophobic core" interaction and serves to present two of the key interacting residues, R10 and W11, to the catalytic residues (Asp197 and Glu233) at the base of the active site. Comparison of the simulated bound state conformation obtained in the docking and the free-state structure calculated from NMR restraints shows that these side chains are relatively well aligned (Figure 4D and S8E). It is worth noting that the docked model and the NMR solution structure independently arrived at this nearly identical turn structure. In contrast to piHA-Dm, the piHA-L26(d14Y) peptide as a whole is observed to be more compact in solution than when bound to its target, increasing from 1787 ± 17 Å^2 solvent-exposed surface area on average in solution to 2179 Å^2 in the docked model (one sample t test $p < 0.0001$) with concomitant loss of the small hydrophobic core. This shows an exchange of intramolecular hydrophobic contacts in the isolated peptide with intermolecular ones in the bound structure, but with maintenance of the same turn structure. Such an effect seems unlikely with a highly rigid structure.

Both solution structures presented here have in common that the few amino acids that form the most important interactions, R10 and W11 for piHA-L26(d14Y) and $^DY1$ and d3 for piHA-Dm(Y 3d), are more ordered in solution, while the remainder of the peptide is more dynamic. This suggests a general binding mode in which the portion that is folded in solution forms an initial interaction with the protein, and this drives the remainder of the peptide to adopt a fold complementary to the surrounding protein surface, acting as a template. Our data also suggests that hydrophobic moieties in side chains and cyclization linkers may be privileged for driving localized folding of these molecules in solution, and thereby improving affinity. The dynamic nature of these noncanonical folds may hold other advantages over rigid canonical folds, such as a better chance of cell-permeability by allowing adoption of alternate conformations that modulate hydrophobicity,[24] or preventing membrane damage through pore formation by amphipathic sequences.[25] These factors should guide future library design for selection of *de novo* macrocyclic peptides. High rigidity or propensity for canonical folds is not necessarily better for strong binding. This also suggests that selection from libraries with multiple fused small cycles may be less successful than a similar number of macrocycles in series, for example as is commonly present in the lanthipeptide family of natural products.[26]

CONCLUSION

Using a combination of crystallography and docking we have shown that macrocyclic peptide inhibitors are able to adopt diverse canonical and noncanonical folds for binding to the same glycosidase active site. We observe a surprising functional convergence of these different scaffolds with one another to present the same motif of two aromatic residues adjacent to a positively charged residue. This motif seems to be particularly privileged for binding to the active site of human pancreatic α-amylase, but it remains to be seen if it can be exploited for binding to other retaining glycosidases. We have also shown that while these noncanonical folds are dynamic in solution, in both examples the amino acids that make the strongest interactions with the target enzyme's active site are stably prefolded, which we propose acts as a primer to drive folding of the rest of the peptide upon association with the protein target. These observations suggest that development of *de novo* macrocyclic peptides should follow a different paradigm to that of their cousins derived from stapling short interacting protein sequences, since constitutive adoption of a canonical fold is not required, or even necessarily beneficial, for high potency.

METHODS

Peptide Synthesis. Peptides were synthesized by automated Fmoc solid phase synthesis on a Biotage (Sweden) Syro II with tentagel S-RAM rink amide resin from Rapp polymere (Germany), then prepared as concentrated stock solutions in DMSO after cleavage, cyclization, and deprotection, as previously described.[16] The noncanonical amino acid L-dopa was incorporated with TBDMS protecting groups on the side chain and deprotected by treatment with TBAF before global deprotection and cleavage with TFA.[27] MALDI-TOF mass spectra were recorded using a Kratos Analytical (UK) Axima-CFR with α-cyano-4-hydroxycinnamic acid as matrix, and UV absorbances were measured with a Thermo Fisher Scientific (USA) Nanodrop 2000. Characterization and purity are detailed in Table S1 and Figure S11.

Enzyme Kinetics. Enzyme kinetics were carried out using purified deglycosylated recombinant human pancreatic α-amylase with the chromogenic substrate 2-chloro-4-nitrophenyl-α-D-maltotrioside from Carbosynth (UK) as previously reported.[13,16] Inhibitors found in an initial screen to have an IC_{50} below 50 nM were characterized using the Morisson method for tight binding inhibitors by varying enzyme as well as inhibitor concentrations,[28] while for all other compounds simple IC_{50} values were determined by varying only inhibitor concentration, up to a maximum of 5 μM. Reported values are ± standard error of fit over all data. Raw data and fitting are shown in Figure S12.

Crystallography. Wild-type human pancreatic α-amylase (HPA) was expressed in *P. pastoris* and isolated as previously described.[29] Co-crystallization of the HPA/piHA-L5(d10Y) complex was performed using the sitting drop vapor diffusion method. Sitting drops were composed in a 1:1 ratio of 2 μL of a solution of 14 mg.mL⁻¹ HPA containing 0.1 M sodium phosphate buffer at pH 7.0 and 2 μL of reservoir solution (54% MPD, 0.1 M Na Cacodylate, pH 7.0). Further, the piHA-L5(d10Y) peptide was introduced into the sitting drop to achieve a saturating concentration. Crystals were incubated at RT and grew up to 3 months to reach full size. For synchrotron data collection, crystals were mounted into nylon cryo-loops (Hampton research) and flash frozen in liquid nitrogen. Crystallization and structure determination of the HPA/piHA-Dm complex has been described previously.[13]

Crystallographic data were collected at cryogenic temperature (100 K) using a PILATUS 6 M detector (Dectris) on beamline BL-12 at the Stanford Synchrotron Radiation Lightsource (Stanford, USA). The diffraction data obtained were indexed and integrated using the program XDS.[30] Data truncation was performed according to a split

half correlation CC(1/2) criterion of 80%[31] and a sigma I/σ cutoff criterion of 2.

To obtain the best possible comparative structural models of the studied HPA ligand complexes an improved structure of wild type HPA was determined at 0.95 Å resolution. This wild-type protein template also served as the search model in the molecular replacement solution for the HPA/piHA-L5(d10Y) complex structure using the program PHASER.[32] Subsequent structural refinement was accomplished by employing the program PHENIX.[33] To confirm peptide binding in the active site of HPA, a simulated annealing Fo − Fc difference electron density omit map was calculated at the 3 sigma level. As is evident in Figure S2, this omit map clearly delineates the bound conformation of the HPA/piHA-L5(d10Y) ligand. Refinement was implemented with default parameters for the HPA/piHA-L5(d10Y) complex but included additional geometry restraints to describe the thioether between the *N*-terminal tyrosine amino acid and the cysteine thiol. Coordinates and restraints for the modified *N*-terminal tyrosine and *C*-terminal amide containing residues were generated using JLigand[34] and added to the peptide chain in the modeling step. Structural refinement was facilitated by iterative model building using the program COOT.[35] After refinement the geometries of the backbone dihedral angles of the piHA-L5(d10Y) complex were distributed within the most favored (98%) and additionally allowed regions (2%) of the Ramachandran map. Further refinement statistics are summarized in the crystal data table (Table S2), with summary of interactions in Table S3. Coordinates and structure factors have been deposited with the PDB under accession codes 5U3A and 5VA9.

Information-Driven Peptide Docking with HADDOCK2.2. Peptide conformations were generated using three different ab initio peptide modeling Web servers, PEPstrMOD,[36] CABS-fold,[37] and Pep-Fold,[38] to which were provided only the primary sequence of piHA-L26 and distance restraints between Y1 and C9, where possible. This yielded 20 peptide models, for which all pairwise root-mean-square-deviations (RMSD), were calculated on the backbone atoms. We then grouped structurally similar peptides using the nearest-neighbor clustering algorithm by Daura et al.[39] In this, peptides were defined as neighbors if their backbone RMSD was below a 2 Å cutoff. The peptide with the largest number of neighbors was eliminated from the pool of peptides together with its neighbors. This step is repeated until no peptides remain in the pool. Upon visual examination of the clusters, we chose the representative peptides of six different clusters as starting conformations for the docking. Since these peptides were still lacking the thioether bridge, an acetyl group was attached to the N-terminus of all six peptides and the cyclization was subsequently achieved by running a short molecular dynamics simulation of 500 steps in explicit solvent using the local version of HADDOCK2.2 to afford the structures given in Figure S5.

For the docking, the receptor of the crystal structure of the HPA/piHA-Dm complex was used (PDB 5KEZ), with prediction of the HPA/piHA-L26 complex achieved with the information-driven docking software HADDOCK (version 2.2)[40] using a standard peptide docking protocol.[41] All peptide residues were treated as passive residues. All receptor residues that are within 5 Å of piHA-Dm in PDB 5KEZ were set as active residues, defining the active site pocket. The resulting models of the HPA/piHA-L26(d14Y) complex were clustered according to the nearest-neighbor algorithm described above using a 5 Å cutoff for the interface RMSD. In the second round of modeling, the same docking protocol was used but incorporating the inhibition data and changing the peptide residues W8 and W11 from passive to active. Docking data are summarized in Figures S13 and S14 as well as Tables S4−S8, and the final optimized model is available as Supporting Information.

NMR Spectroscopy and Structure Determination. Unlabeled 0.5 mM piHA-Dm(Y 3d) and 0.5 mM piHA-L26(d14Y) were dissolved in 130 mM NaCl, 25 mM NaPi pH 6.5, 0.01% NaN₃, and 10% D_2O NMR sample buffer. Homonuclear ¹H−¹H 2D NOESY (200 ms mixing time), 2D TOCSY (40 ms mixing time), 2D COSY-DQF, and 2D ¹³C−¹H HSQC (only aliphatic region for piHA-L26(d14Y) spectra) were recorded at 293 K on a 600 MHz Bruker Avance NMR Spectrometer equipped with a cryogenic probe, for

both samples. Typical acquisition times were 20−50 ms in t_1, 80−280 ms in t_2, and a total acquisition time of 11−40 h. Spectral processing was performed using Topspin.

^{1}H assignment was carried out using sequential walk[42] based on conventional 2D TOCSY and 2D NOESY spectra, as well as 2D COSY-DQF for regiospecific aromatic assignments and 2D ^{13}C-HSQC for acetyl linker methylene nuclei as well as ^{13}C chemical shifts (Figure S15−S17). Side chain and C-terminal amides were assigned stereospecifically as described by Harsch et al.[43] For assignment and analysis of the spectra, NMRFAM-Sparky[44] was used. ^{13}C chemical shift referencing was adjusted by 2.66 ppm compared to standard Bruker referencing, as described by Aeschbacher et al.[45] S2 order parameters were predicted from ^{1}Hα, ^{1}HN, ^{13}Cα, and ^{13}Cβ chemical shifts using the TALOS+ web server;[46] secondary structure propensities were predicted using the SSP software.[47] $^3J_{HNHα}$ coupling constants were determined from HN−Hα antiphase cross peaks in a 2D COSY-DQF spectrum, recorded as described above. To ensure sufficient resolution for peak fitting, t_{2max} was 277 ms, zero filling was applied to a digital resolution below 0.5 Hz/point, and spectra were processed to obtain full Lorentzian line shape. Antiphase multiplets were fit exclusively in the direct dimension to obtain sufficient resolution and only on signals detected on HN due to coupling of Hα with Hβ, which causes additional splitting. A MATLAB function was written to fit two Lorentzian peaks of opposite sign to the antiphase doublet, thereby obtaining the ^{3}J coupling constant from the peak separation. Doublets were fit with a constant peak intensity and line width for both peaks, unless a model with different peak intensity and line width for both peaks was a statistically significantly better fit ($p < 0.05$), as assessed using a chi-square difference test. In case the signal-to-noise ratio of separate doublets was insufficient to accurately fit an antiphase Lorentzian doublet, the two antiphase doublets making up the antiphase quartet in the 2D spectrum were added to increase the signal-to-noise ratio.

Structure calculations were performed by restrained torsion angle dynamics using CYANA,[48] starting from 200 randomly generated initial conformations and selecting the 20 lowest energy conformers after 10 000 steps. Subsequently, structures were refined by restrained Cartesian dynamics in explicit TIP3P water in CNS 1.2,[49] according to the following procedure based on the RECOORD protocol:[50] an initial 120 step energy minimization in explicit water, followed by stepwise heating from 100 to 300 K in 50 K steps (200 MD steps of 3 fs per temperature), 2000 MD steps of 4 fs at 300 K, stepwise cooling to 25 K with temperature steps of 25 K (200 MD steps of 4 fs), and finally 200 steps of energy minimization. The CYANA and CNS residue libraries were adapted to incorporate non-natural amino acids and peptide cyclization. Proline trans conformation was confirmed for both peptides using Cβ and Cγ chemical shifts and NOE signals, as described in literature.[51]

Distance restraints were automatically calibrated from NOE peak volumes by CYANA using a reference distance of 5 Å for piHA-Dm(Y 3d) and 6 Å for piHA-L26(d14Y), as the NOEs for the latter peptide were more medium to long-range than for the other peptide and this reference distance allowed some flexibility in these longer range contacts as well. The maximum restraint used was 7 Å. Distances were corrected automatically for the lack of stereospecific assignments in diastereotopic groups. $^3J_{HNHα}$ coupling constants significantly greater than 8 Hz were converted to φ angle torsional restraints of −120 ± 40°, as determined using the Karplus equation,[52] accommodating rotational averaging to a certain degree. $^3J_{HNHα}$ coupling constants in the range of 6−8 Hz were not converted into torsional restraints, as these values are often associated with rotational averaging.[53] TALOS+ predictions which were marked as "good" for residues with an order parameter greater than 0.65, as recommended for nonrigid structures, were converted into φ and ψ angle torsional restraints of predicted angle ±2 × standard deviation to allow for limited flexibility and approximate the 95% confidence interval of the prediction. TALOS+ prediction for Pro2 of piHA-Dm(Y 3d) was not included as a torsional restraint, as it caused a significant increase in Ramachandran clashes. The input restraints are summarized in Table S10. Structure quality was assessed using PROCHECK.[54]

■ ASSOCIATED CONTENT

Ⓢ Supporting Information

The Supporting Information is available free of charge on the ACS Publications website at DOI: 10.1021/acschembio.9b00290.

> Supplementary methods on crystallography, Figures S1−S17, Tables S1−S10 (PDF)
>
> Final amylase-docked model of peptide piHA-L26-Δ14 (PDB)

■ AUTHOR INFORMATION

Corresponding Author
*Email: s.a.k.jongkees@uu.nl.

ORCID ⓘ
Bram J. A. Vermeulen: 0000-0002-9798-6245
Alexandre M. J. J. Bonvin: 0000-0001-7369-1322
Seino A. K. Jongkees: 0000-0002-4796-0557

Author Contributions
#These authors contributed equally.

Notes
The authors declare no competing financial interest.

■ ACKNOWLEDGMENTS

■ REFERENCES

(1) Pelay-Gimeno, M., Glas, A., Koch, O., and Grossmann, T. N. (2015) Structure-Based Design of Inhibitors of Protein-Protein Interactions: Mimicking Peptide Binding Epitopes. *Angew. Chem., Int. Ed. 54*, 8896−8927.

(2) Luther, A., Moehle, K., Chevalier, E., Dale, G., and Obrecht, D. (2017) Protein Epitope Mimetic Macrocycles as Biopharmaceuticals. *Curr. Opin. Chem. Biol. 38*, 45−51.

(3) Gao, M., Cheng, K., and Yin, H. (2015) Targeting Protein-Protein Interfaces Using Macrocyclic Peptides. *Biopolymers 104*, 310−316.

(4) Huang, Y., Wiedmann, M. M., and Suga, H. (2018) RNA Display Methods for the Discovery of Bioactive Macrocycles. *Chem. Rev.*, DOI: 10.1021/acs.chemrev.8b00430.

(5) Jongkees, S. A. K., Hipolito, C. J., Rogers, J. M., and Suga, H. (2015) Model Foldamers: Applications and Structures of Stable Macrocyclic Peptides Identified Using in Vitro Selection. *New J. Chem. 39*, 3197−3207.

(6) Otero-Ramirez, M., Passioura, T., and Suga, H. (2018) Structural Features and Binding Modes of Thioether-Cyclized Peptide Ligands. *Biomedicines* 6, 116.

(7) Song, X., Lu, L., Passioura, T., and Suga, H. (2017) Macrocyclic Peptide Inhibitors for the Protein - Protein Interaction of Zaire Ebola Virus Protein 24 and Karyopherin Alpha 5. *Org. Biomol. Chem. 15*, 5155–5160.

(8) Ito, K., Sakai, K., Suzuki, Y., Ozawa, N., Hatta, T., Natsume, T., Matsumoto, K., and Suga, H. (2015) Artificial Human Met Agonists Based on Macrocycle Scaffolds. *Nat. Commun. 6*, 6373.

(9) Morimoto, J., Hayashi, Y., and Suga, H. (2012) Discovery of Macrocyclic Peptides Armed with a Mechanism-Based Warhead: Isoform-Selective Inhibition of Human Deacetylase SIRT2. *Angew. Chem., Int. Ed. 51*, 3423–3427.

(10) Hayashi, Y., Morimoto, J., and Suga, H. (2012) In Vitro Selection of Anti-Akt2 Thioether-Macrocyclic Peptides Leading to Isoform-Selective Inhibitors. *ACS Chem. Biol. 7*, 607–613.

(11) Lau, Y. H., de Andrade, P., Wu, Y., and Spring, D. R. (2015) Peptide Stapling Techniques Based on Different Macrocyclisation Chemistries. *Chem. Soc. Rev. 44*, 91–102.

(12) Azzarito, V., Long, K., Murphy, N., and Wilson, A. (2013) Inhibition of Alpha-Helix-Mediated Protein-Protein Interactions Using Designed Molecules. *Nat. Chem. 5*, 161–173.

(13) Jongkees, S. A. K., Caner, S., Tysoe, C., Brayer, G. D., Withers, S. G., and Suga, H. (2017) Rapid Discovery of Potent and Selective Glycosidase-Inhibiting de Novo Peptides. *Cell Chem. Biol. 24*, 381–390.

(14) Passioura, T., and Suga, H. (2017) A RaPID Way to Discover Nonstandard Macrocyclic Peptide Modulators of Drug Targets. *Chem. Commun. 53*, 1931–1940.

(15) Williams, L. K., Zhang, X., Caner, S., Tysoe, C., Nguyen, N. T., Wicki, J., Williams, D. E., Coleman, J., McNeill, J. H., Yuen, V., Andersen, R. J., Withers, S. G., and Brayer, G. D. (2015) The Amylase Inhibitor Montbretin A Reveals a New Glycosidase Inhibition Motif. *Nat. Chem. Biol. 11*, 691–696.

(16) Yoshisada, R., van Gijzel, L., and Jongkees, S. A. K. K. (2017) Towards a Tuneable Retaining Glycosidase Inhibition Motif by Mimicry of a Plant Flavonol Warhead. *ChemBioChem 18*, 2333–2339.

(17) Kodan, A., Yamaguchi, T., Nakatsu, T., Sakiyama, K., Hipolito, C. J., Fujioka, A., Hirokane, R., Ikeguchi, K., Watanabe, B., Hiratake, J., Kimura, Y., Suga, H., Ueda, K., and Kato, H. (2014) Structural Basis for Gating Mechanisms of a Eukaryotic P-Glycoprotein Homolog. *Proc. Natl. Acad. Sci. U. S. A. 111*, 4049–4054.

(18) Hipolito, C. J., Bashiruddin, N. K., and Suga, H. (2014) Protein Cocrystallization Molecules Originating from in Vitro Selected Macrocyclic Peptides. *Curr. Opin. Struct. Biol. 26*, 24–31.

(19) De Vries, S. J., Van Dijk, M., and Bonvin, A. M. J. J. (2010) The HADDOCK Web Server for Data-Driven Biomolecular Docking. *Nat. Protoc. 5*, 883–897.

(20) Wiegand, G., Epp, O., and Huber, R. (1995) The Crystal Structure of Porcine Pancreatic α-Amylase in Complex with the Microbial Inhibitor Tendamistat. *J. Mol. Biol. 247*, 99–110.

(21) Vértesy, L., Oeding, V., Bender, R., Zepf, K., and Nesemann, G. (1984) Tendamistat (HOE 467), a Tight-Binding α-Amylase Inhibitor from Streptomyces Tendae 4158. Isolation, Biochemical Properties. *Eur. J. Biochem. 141*, 505–512.

(22) Etzkorn, F. A., Guo, T., Lipton, M. A., Goldberg, S. D., and Bartlett, P. A. (1994) Cyclic Hexapeptides and Chimeric Peptides as Mimics of Tendamistat. *J. Am. Chem. Soc. 116*, 10412–10425.

(23) Sefler, A. M., Kozlowski, M. C., Guo, T., and Bartlett, P. A. (1997) Design, Synthesis, and Evaluation of a Depsipeptide Mimic of Tendamistat. *J. Org. Chem. 62*, 93–102.

(24) Deshayes, S., Decaffmeyer, M., Brasseur, R., and Thomas, A. (2008) Structural Polymorphism of Two CPP: An Important Parameter of Activity. *Biochim. Biophys. Acta, Biomembr. 1778*, 1197–1205.

(25) Su, Y., Mani, R., Doherty, T., Waring, A. J., and Hong, M. (2008) Reversible Sheet-Turn Conformational Change of a Cell-Penetrating Peptide in Lipid Bilayers Studied by Solid-State NMR. *J. Mol. Biol. 381*, 1133–1144.

(26) Willey, J. M., and van der Donk, W. A. (2007) Lantibiotics: Peptides of Diverse Structure and Function. *Annu. Rev. Microbiol. 61*, 477–501.

(27) Sever, M. J., and Wilker, J. J. (2001) Synthesis of Peptides Containing DOPA (3,4-Dihydroxyphenylalanine). *Tetrahedron 57*, 6139–6146.

(28) Morrison, J. F. (1969) Kinetics of the Reversible Inhibition of Enzyme-Catalysed Reactions by Tight-Binding Inhibitors. *Biochim. Biophys. Acta 185*, 269–286.

(29) Rydberg, E. H., Sidhu, G., Vo, H. C., Hewitt, J., Côté, H. C. F., Wang, Y., Numao, S., Gillivray, R. T. A. M., Overall, C. M., Brayer, G. D., and Withers, S. G. (1999) Cloning, Mutagenesis, and Structural Analysis of Human Pancreatic α-Amylase Expressed in Pichia Pastoris. *Protein Sci. 8*, 635–643.

(30) Kabsch, W. (2010) XDS. *Acta Crystallogr., Sect. D: Biol. Crystallogr. 66*, 125–132.

(31) Karplus, P. A., and Diedrichs, K. (2012) Linking Crystallographic Model and Data Quality. *Science 336*, 1030–1033.

(32) McCoy, A. J. (2007) Solving Structures of Protein Complexes by Molecular Replacement with Phaser. *Acta Crystallogr., Sect. D: Biol. Crystallogr. 63*, 32–41.

(33) Adams, P. D., Afonine, P. V., Bunkóczi, G., Chen, V. B., Davis, I. W., Echols, N., Headd, J. J., Hung, L. W., Kapral, G. J., Grosse-Kunstleve, R. W., McCoy, A. J., Moriarty, N. W., Oeffner, R., Read, R. J., Richardson, D. C., Richardson, J. S., Terwilliger, T. C., and Zwart, P. H. (2010) PHENIX: A Comprehensive Python-Based System for Macromolecular Structure Solution. *Acta Crystallogr., Sect. D: Biol. Crystallogr. 66*, 213–221.

(34) Lebedev, A. A., Young, P., Isupov, M. N., Moroz, O. V., Vagin, A. A., and Murshudov, G. N. (2012) JLigand: A Graphical Tool for the CCP4 Template-Restraint Library. *Acta Crystallogr., Sect. D: Biol. Crystallogr. 68*, 431–440.

(35) Emsley, P., and Cowtan, K. (2004) Coot: Model-Building Tools for Molecular Graphics. *Acta Crystallogr., Sect. D: Biol. Crystallogr. D60*, 2126–2132.

(36) Singh, S., Singh, H., Tuknait, A., Chaudhary, K., Singh, B., Kumaran, S., and Raghava, G. P. S. (2015) PEPstrMOD: Structure Prediction of Peptides Containing Natural, Non-Natural and Modified Residues. *Biol. Direct 10*, 73.

(37) Kolinski, A. (2004) Protein Modeling and Structure Prediction with a Reduced Representation. *Acta Biochim. Polonica 51*, 349.

(38) Shen, Y., Maupetit, J., Derreumaux, P., and Tufféry, P. (2014) Improved PEP-FOLD Approach for Peptide and Miniprotein Structure Prediction. *J. Chem. Theory Comput. 10*, 4745–4758.

(39) Daura, X., Gademann, K., Jaun, B., Seebach, D., van Gunsteren, W. F., and Mark, A. E. (1999) Peptide Folding: When Simulation Meets Experiment. *Angew. Chem., Int. Ed. 38*, 236–240.

(40) Van Zundert, G. C. P., Rodrigues, J. P. G. L. M., Trellet, M., Schmitz, C., Kastritis, P. L., Karaca, E., Melquiond, A. S. J., Van Dijk, M., De Vries, S. J., and Bonvin, A. M. J. J. (2016) The HADDOCK2.2 Web Server: User-Friendly Integrative Modeling of Biomolecular Complexes. *J. Mol. Biol. 428*, 720–725.

(41) Trellet, M., Melquiond, A. S. J., and Bonvin, A. M. J. J. (2015) Information-Driven Modeling of Protein-Peptide Complexes. *Methods Mol. Biol. 1268*, 221.

(42) Hosur, R. V., Wider, G., and Wüthrich, K. (1983) Sequential Individual Resonance Assignments in the 1H Nuclear-Magnetic-Resonance Spectrum of Cardiotoxin VII 2 from Naju Mossambica Rnossumbica. *Eur. J. Biochem. 130*, 497–508.

(43) Harsch, T., Schneider, P., Kieninger, B., Donaubauer, H., and Kalbitzer, H. R. (2017) Stereospecific Assignment of the Asparagine and Glutamine Sidechain Amide Protons in Proteins from Chemical Shift Analysis. *J. Biomol. NMR 67*, 157–164.

(44) Lee, W., Tonelli, M., and Markley, J. L. (2015) NMRFAM-SPARKY: Enhanced Software for Biomolecular NMR Spectroscopy. *Bioinformatics 31*, 1325–1327.

(45) Aeschbacher, T., Schubert, M., and Allain, F. H.-T. (2012) A Procedure to Validate and Correct the 13C Chemical Shift Calibration of RNA Datasets. *J. Biomol. NMR 52*, 179−190.

(46) Shen, Y., Delaglio, F., Cornilescu, G., and Bax, A. (2009) TALOS+: A Hybrid Method for Predicting Protein Backbone Torsion Angles from NMR Chemical Shifts. *J. Biomol. NMR 44*, 213−223.

(47) Marsh, J. A., Singh, V. K., Jia, Z., and Forman-Kay, J. D. (2006) Sensitivity of Secondary Structure Propensies to Sequence Differences between Alpha- and Gamma-Synuclein: Implications for Fibrillation. *Protein Sci. 15*, 2795−2804.

(48) Güntert, P., and Buchner, L. (2015) Combined Automated NOE Assignment and Structure Calculation with CYANA. *J. Biomol. NMR 62*, 453−471.

(49) Brunger, A. T. (2007) Version 1.2 of the Crystallography and NMR System. *Nat. Protoc. 2*, 2728−2733.

(50) Nederveen, A. J., Doreleijers, J. F., Vranken, W., Miller, Z., Spronk, C. A. E. M., Nabuurs, S. B., Güntert, P., Livny, M., Markley, J. L., Nilges, M., Ulrich, E. L., Kaptein, R., and Bonvin, A. M. J. J. (2005) RECOORD: A Recalculated Coordinate Database of 500+ Proteins from the PDB Using Restraints from the BioMagResBank. *Proteins: Struct., Funct., Genet. 59*, 662−672.

(51) Schubert, M., Labudde, D., Oschkinat, H., and Schmieder, P. (2002) A Software Tool for the Prediction of Xaa-Pro Peptide Bond Conformations in Proteins Based on 13 C Chemical Shift Statistics. *J. Biomol. NMR 24*, 149−154.

(52) Wang, A. C., and Bax, A. (1996) Determination of the Backbone Dihedral Angles φ in Human Ubiquitin from Reparametrized Empirical Karplus Equations. *J. Am. Chem. Soc. 118*, 2483−2494.

(53) Cavanagh, J., Fairbrother, W. J., Palmer, A. G. I., and Skelton, N. J. (2007) *Protein NMR Spectroscopy: Principles and Practice*; Academic Press.

(54) Laskowski, R. A., MacArthur, M. W., Moss, D. S., and Thornton, J. M. (1993) IUCr. PROCHECK: A Program to Check the Stereochemical Quality of Protein Structures. *J. Appl. Crystallogr. 26*, 283−291.